Electrochemical Control over Photoinduced Electron Transfer and Trapping in CdSe-CdTe Quantum-Dot Solids

Simon C. Boehme,[†] T. Ardaan Walvis,[†] Ivan Infante,[‡] Ferdinand C. Grozema,[†] Daniël Vanmaekelbergh,[§] Laurens D. A. Siebbeles,[†] and Arjan J. Houtepen[†,*]

[†]Chemical Engineering, Optoelectronic Materials, TU Delft, Julianalaan 136, 2628 BL Delft, The Netherlands, [‡]Kimika Fakultatea, Euskal Herriko Unibertsitatea (UPV/EHU) and Donostia International Physics Center (DIPC), P.K. 1072 Donostia, Euskadi, Spain, and [§]Debye Institute, Condensed Matter and Interfaces, Utrecht University, P.O. Box 80.000, 3508 TA Utrecht, The Netherlands. S.C.B. and T.A.W. performed the experiments. A.J.H. conceived and supervised the experiments. I.I., F.C.G, D.V., and L.D.A.S. gave advice on experiments and interpretation. S.C.B. and A.J.H. wrote the manuscript. All authors commented on the manuscript and approved the final version.

ABSTRACT Understanding and controlling charge transfer between different kinds of colloidal quantum dots (QDs) is important for devices such as light-emitting diodes and solar cells and for thermoelectric applications. Here we study photoinduced electron transfer between CdTe and CdSe QDs in a QD film. We find that very efficient electron trapping in CdTe QDs obstructs electron transfer to CdSe QDs under most conditions. Only the use of thiol ligands results in somewhat slower electron trapping; in this case the competition between trapping and electron transfer results in a small fraction of electrons being transferred to CdSe. However, we demonstrate that electron trapping can be controlled and even avoided altogether by using the unique combination of electrochemistry and transient absorption spectroscopy. When the Fermi level is raised electrochemically, traps are filled with electrons and electron transfer from CdTe to CdSe QDs occurs with unity efficiency. These results show the great importance of knowing and controlling the Fermi level in QD films and open up the possibility of studying the density of trap states in QD films as well as the systematic investigation of the intrinsic electron transfer rates in donor–acceptor films.

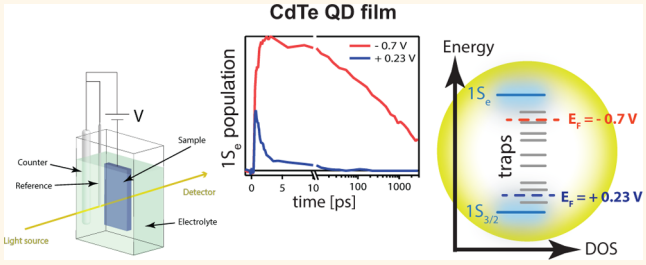

KEYWORDS: quantum dot · defect · trapping · charge transfer · Fermi level · electrochemistry · ligands · transient absorption spectroscopy

Charge transfer lies at the heart of operation of many devices, such as LEDs, solar cells, thermoelectrics and photoelectrochemical solar fuel cells. In all such devices colloidal semiconductor quantum dots (QDs) are investigated as electron donors and/or acceptors.[1,2] Understanding the fundamental laws governing the charge transfer process between QDs is therefore a key to further advances in these devices. Various studies have been conducted to reveal the efficiency and rate of charge transfer processes in QDs in solution or attached to a semiconductor surface.[3−10] Parameters that commonly determine the rate of charge transfer are the driving force between donor and acceptor,[10] the width and height of an energy barrier, given by the distance and energy landscape between donor and acceptor, respectively,[6] and by the dielectric environment.[10] However, the efficiency of charge transfer is not just influenced by the charge transfer rate, but also by the rate of competing processes. The initial aim of this study was to study electron transfer from CdTe to CdSe QDs since these materials are known to form a type II band offset.[11−14] However, we found that sub-picosecond electron trapping in CdTe QDs obstructs electron transfer to CdSe QDs. Therefore, we first performed a systematic investigation of the trapping processes in CdTe QDs and then set out to reduce the trapping rates and to allow charge transfer to CdSe QDs to occur. We demonstrate that thiol ligands reduce the

* Address correspondence to a.j.houtepen@tudelft.nl.

Received for review April 9, 2014 and accepted June 2, 2014.

Published online June 02, 2014
10.1021/nn501985e

electron-trapping rate sufficiently, albeit only just, for electron transfer to take place. However, full control over charge trapping and charge transfer is enabled by applying an electrochemical potential to the QD films. This allows filling of trap states, thereby switching off electron trapping and enabling electron transfer from CdTe to CdSe QDs.

RESULTS AND DISCUSSION

CdTe and CdSe QDs between 3 and 6 nm were synthesized according to reported recipes.[15,16] The organic ligands on the QD surface are oleic acid (OA) and trioctylphosphine (TOP) for CdTe QDs and hexadecylamine (HDA), trioctylphosphine (TOP), trioctylphosphine oxide (TOPO) and tetradecylphosphonic acid (TDPA) for CdSe QDs. Figure 1a shows absorption and emission spectra of dispersions of the synthesized QDs.

Photoconductive films of these QDs on quartz or indium doped tin oxide (ITO) substrates were prepared with a layer-by-layer (LbL) dip coating process in a N_2 purged glove box; see Experimental Section for details. The long insulating ligands that result from the QD synthesis are replaced by shorter bidentate ligands, either 1,2-ethanediamine (2DA), 1,2-ethanedithiol (2DT) or oxalic acid (2DAc). Whereas they differ in their functional group, all of these new ligands contain only two carbon atoms as a "spacer". These shorter ligands are intended to increase the electronic coupling between QDs.[17]

As stated above, the aim of this work is to study charge transfer between CdTe and CdSe QDs. Figure 1b shows a schematic of the band alignment between CdTe and CdSe QDs. For common QD sizes, these materials are expected to form a type II band alignment with both HOMO and LUMO levels of CdSe at a lower energy than the levels in CdTe.[11−14] This is the case for all combinations of sizes in Figure 1a, in spite of large differences in their band gap. Hence, upon photoexcitation of CdTe QDs, electron transfer to CdSe QDs could take place. To reveal the time dependent population of electrons in CdTe and CdSe QDs, we measure the time and energy dependent change in absorption $\Delta A(E,t) = A^*(E,t) - A(E)$ between the excited (A^*) and unexcited (A) sample in broadband transient absorption (TA) measurements. As shown in the Supporting Information, this change in absorption allows to deduce the density of excitations per unit area $N^*(t)$ *via*

$$\Delta A(E,t) = \sigma^*(E) \cdot N^*(t) / \ln 10 \qquad (1)$$

where the cross section of a single excitation $\sigma^*(E)$ is derived from the signal at time zero according to

$$\sigma^*(E) = \frac{\Delta A(E, t = 0) \cdot \ln 10}{I_0 \cdot F_A} \qquad (2)$$

with I_0 the excitation fluence and F_A the fraction of absorbed pump light, obtained by measuring the transmission through the QD film in an integrating sphere, thereby correcting for reflection and scattering.

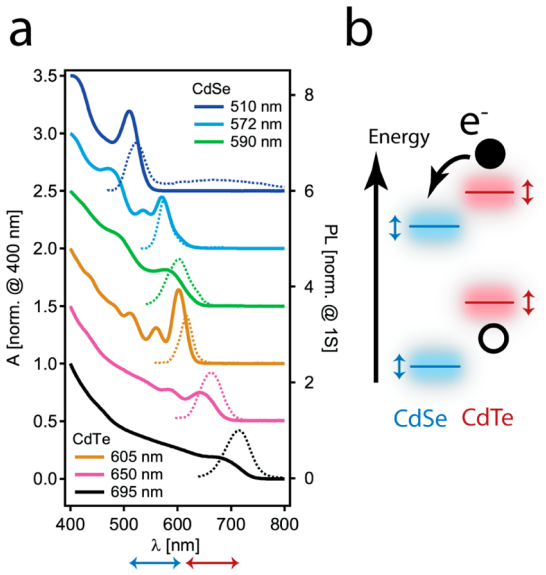

Figure 1. (a) Absorption spectra (solid lines, *versus* left axis) and photoluminescence (PL) spectra (dotted lines, *versus* right axis) of CdSe and CdTe QDs in dispersion with diameters ranging from 3 to 6 nm. Absorption spectra are normalized at 400 nm and PL spectra at their respective $1S_{3/2}1S_e$ peak. Spectra are offset for clarity. The $1S_{3/2}1S_e$ absorption peak wavelengths are denoted in the legend. (b) Schematic of electron transfer from CdTe to CdSe QDs due to the type II band alignment[11−14] that is expected for all combinations of CdSe and CdTe QDs displayed in (a). Blue and red arrows schematically indicate size dependent variations in QD band gap and, hence, energy level alignment.

In this work we display excitation density normalized transient absorption data as $(\Delta A(E,t))/(I_0 F_A)$. At time zero, this "absorption bleach per excitation" is directly related to the cross section per excitation $\sigma^*(E)$ *via* eq 2. For all later times, it shows the decay of excitations according to eq 1. Electron transfer in films containing CdTe donor and CdSe acceptor QDs can be inferred from an increasing absorption bleach at the CdSe $1S_{3/2}1S_e$ transition and can be quantified by first determining $\sigma^*(E)$ for individual CdSe and CdTe QD films.

Initial TA measurements on films that contained CdTe donor QDs (either 3.7 or 6.3 nm in diameter) and CdSe acceptor QDs (4.1 nm in diameter), both capped with 2DA ligands, did not show any signals belonging to the acceptors, indicating that negligible electron transfer took place. Instead, only a very short-lived bleach of the $1S_{3/2}1S_e$ transition in the CdTe QDs was observed, which decayed on a time scale of a picosecond. We hypothesized that this is due to fast electron trapping in CdTe QDs. If this trapping is much faster than the electron transfer time to CdSe QDs, no donor−acceptor signal will be observed.

TA measurements on various CdTe QD dispersions are presented in the Supporting Information. They show two important characteristics: (1) the bleach of the $1S_{3/2}1S_e$ transition is due to $1S_e$ electrons only. The presence of a $1S_{3/2}$ hole results in a much smaller bleach, if any, than the presence of a $1S_e$ electron. This is in line

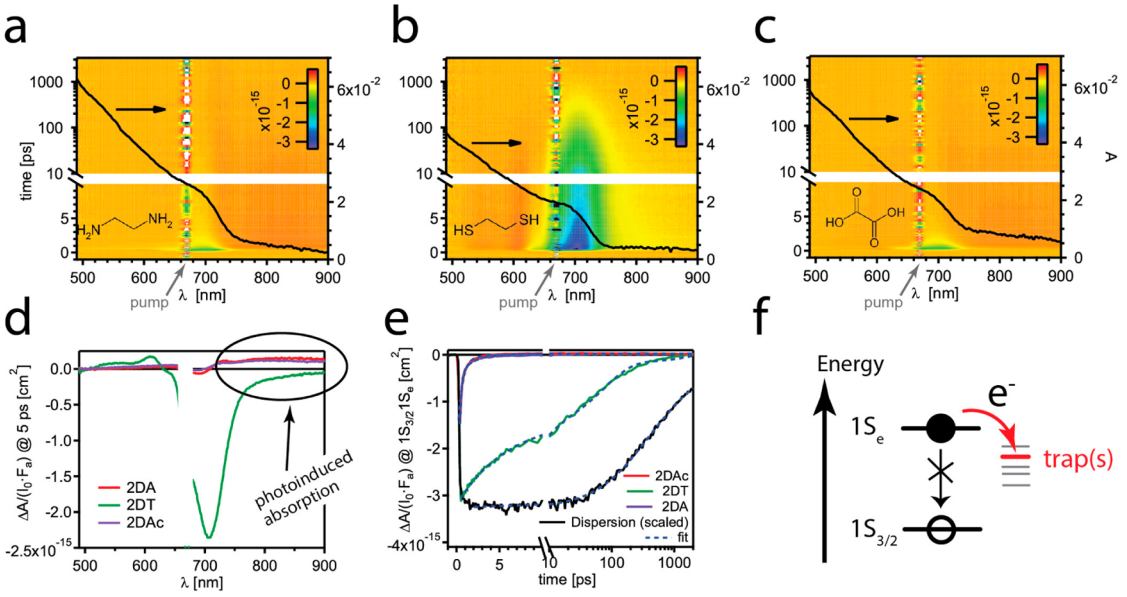

Figure 2. Effect of ligand anchor group on electron trapping behavior: 2D TA image displaying the bleach per excitation $\Delta A/(I_0F_A)$ for films of 6.3 nm CdTe QDs capped with 2DA (a), 2DT (b), and 2DAc (c) after excitation at 670 nm. The linear absorption spectra are plotted *versus* the right axis. The pump wavelength is indicated with grey arrows. (d) Transient absorption spectra at 5 ps pump-probe delay. (e) Kinetics of the $1S_{3/2}1S_e$ bleach, together with triexponential fits (see main text). (f) Sketch of the proposed electron trapping process.

with previous work from the Klimov[18] and Kambhampati groups,[19] and has been attributed to the higher degeneracy of the $1S_{3/2}$ hole level compared to the $1S_e$ electron level in cadmium chalcogenides.[20] Therefore, we will assume here that the kinetics of the $1S_{3/2}1S_e$ bleach represent the kinetics of $1S_e$ electrons and that any fast decay of this signal is due to electron trapping. At the end of this report, we present experimental evidence for this assignment using electrochemical control of the Fermi level. (2) We observe large sample-to-sample variations in the rate of electron trapping. We find for instance that the rate of electron trapping increases with increased number of washing steps in the purification of the QD dispersions. This is consistent with a report by Morris-Cohen *et al.*[21] who observed a loss of ligands and a drop in PL quantum yield during purification. Such a loss of ligands may result in a higher number of traps on the QD surface.

Fast Electron Trapping in CdTe QD Films. We prepared films of 6.3 nm CdTe QDs *via* layer-by-layer dipcoating, during which the original oleic acid ligands are exchanged for 1,2-ethanediamine (2DA), 1,2-ethanedithiol (2DT) or oxalic acid (2DAc). The decreased distance between QDs results in enhanced electronic coupling as evidenced by a much increased photoconductivity.[14,22]

The films with 2DA, 2DT and 2DAc ligands are excited at 670 nm, at the blue edge of their $1S_{3/2}1S_e$ transition, with ~180 fs pulses at a fluence of 2.5×10^{13} photons per cm^2, a FWHM of 8 nm and at a repetition rate of 2500 Hz. Transient absorption spectra of the samples are recorded with a broadband probe pulse of ~180 fs at a repetition rate of 5000 Hz, as a function of time delay with respect to the pump pulse. This yields the 2D TA images shown in Figures 2a–c for films with 2DA, 2DT and 2DAc ligands, respectively. The bleach per excitation $\Delta A/(I_0F_A)$ is shown in false colors. To better resolve both fast and slow dynamics, the time axis is displayed on a linear scale from −1 to 10 ps and on a logarithmic scale from 10 to 3000 ps. The linear absorption spectra are displayed as black solid lines *versus* the right axis. The image has been corrected for dispersion of the probe light as outlined in the Supporting Information. For all TA data in the remainder of this document similar excitation conditions are ensured with fluences on the order of 10^{13} photons per cm^2, leading to an average of 0.1 excitations per QD. The exact fluence for each data set is given in Table S1 (Supporting Information).

The dominant feature is an absorption bleach of the $1S_{3/2}1S_e$ transition around 700 nm, indicative of charges populating the $1S_{3/2}$ hole and/or $1S_e$ electron state. However, the population persists only for a short time: for 2DA and 2DAc ligands, its picosecond decay is three orders of magnitude faster than for the same QDs with the original ligands in dispersion (see Figure S2d,a,c, Supporting Information). Only 2DT ligands lead to a slightly longer lifetime (see Figure 2b). A comparison of the $1S_{3/2}1S_e$ bleach kinetics of the three films as well as the dispersion with the original ligands is shown in Figure 2e.

For all samples, the decay must be nonradiative in nature, as the observed kinetics are much faster than the reported radiative lifetime of 38.8 ns for CdTe QDs of this size.[23] The decay could hence be due to electron trapping, or nonradiative electron-hole recombination. We discard Auger recombination as the major decay

TABLE 1. Overview of Lifetimes Obtained from a Triexponential Fit to the TA Decays at the $1S_{3/2}1S_e$ Transition[a]

					lifetimes [ps]		
material	diameter [nm]	ligands	state	material probed	τ_1	τ_2	τ_3 (fixed)[23]
CdTe	3.7	TOP, oleic acid	dispersion ($CHCl_3$)	CdTe	$2.8 \pm 0.1^{(trap)}$	$46 \pm 2^{(trap)}$	$22\,200^{(rad)}$
CdTe	6.3	TOP, oleic acid	dispersion ($CHCl_3$)	CdTe	$192 \pm 34^{(trap)}$	$942 \pm 301^{(trap)}$	$38\,800^{(rad)}$
CdTe	6.3	2DA	film	CdTe	$< 0.2^{(trap)}$	$1.6 \pm 0.1^{(trap)}$	$38\,800^{(rad)}$
CdTe	6.3	2DAc	film	CdTe	$< 0.2^{(trap)}$	$3.1 \pm 2.1^{(trap)}$	$38\,800^{(rad)}$
CdTe	6.3	2DT	film	CdTe	$5.3 \pm 0.2^{(trap)}$	$76 \pm 3^{(trap)}$	$38\,800^{(rad)}$
CdSe/CdTe	4.1/6.3	2DT	film	CdSe	$2.9 \pm 0.1^{(trans)}$	$327 \pm 20^{(trap)}$	$26\,000^{(rad)}$
CdSe/CdTe	4.1/6.3	2DT	film	CdTe	$0.22 \pm 0.01^{(trap)}$	$2.4 \pm 0.1^{(trans)}$	–
CdSe/CdTe	4.1/6.3	2DA	film	CdSe	$0.23 \pm 0.01^{(trans)}$	$2.3 \pm 0.3^{(trans)}$	$26\,000^{(rad)}$
CdSe/CdTe	4.1/6.3	2DA	film	CdTe	$0.23 \pm 0.01^{(trans)}$	$2.3 \pm 0.3^{(trans)}$	$38\,800^{(rad)}$

[a] Assignments of lifetimes to either electron trapping, electron transfer or radiative recombination are indicated with the $^{(trap)}$, $^{(trans)}$ and $^{(rad)}$, respectively.

mechanism, as typical Auger lifetimes are on the order of tens to hundreds of picoseconds[24] and thus longer than our observed decay. Consequently, we identify electron trapping as the origin of the fast decay of the $1S_{3/2}1S_e$ bleach.

The $1S_{3/2}1S_e$ decay kinetics of the CdTe QD dispersions and films are well described by a triexponential function of the form $\Delta A(t) = \sum_i c_i \cdot \exp(-t/\tau_i)$, where $i = 1, 2, 3$ and c_i and τ_i are the amplitudes and lifetimes of the exponential components. The fits are displayed as blue dashed lines in Figure 2e. We chose $\tau_3 = 38.8$ ns to match the radiative lifetime,[23] and left all other parameters free. The fit parameters are shown in Table 1. In addition to the radiative decay, at least two components are required for a good fit. This suggests that two types of traps must be present. The assignment of the lifetimes τ_1 and τ_2 to specific surface sites is of great interest, but is beyond the scope of this work. We will discuss the nature of these traps in a forthcoming publication.

For the 2DT capped film $\tau_1 = 5.3 \pm 0.2$ ps and $\tau_2 = 76 \pm 3$ ps best describe the data. The diamine and diacid capped films feature significantly shorter lifetimes: the slower component is $\tau_2 = 1.6 \pm 0.1$ ps for 2DA and 3.1 ± 2.1 ps for 2DAc, respectively, while the fast component (τ_1) even falls short of our instrument response time, for both ligands. This sets an upper limit $\tau_1 \leq 0.2$ ps for 2DA and 2DAc. Significant decay during the pump pulse is also the reason why the bleach magnitude for films with these ligands is lower than for films with 2DT ligands.

Even for the QD film with dithiol ligands, the observed kinetics are three orders of magnitude faster than the radiative decay (see Table 1). Apparently, the preparation of conductive QD films has resulted in the introduction of very efficient electron traps. We further point out that for the 2DA and 2DAc capped films, the lifetimes are even shorter than typical cooling times. Since trapping competes with electron cooling, high energy excitation results in a small $1S_e$ population per incident photon (see Figure S3, Supporting Information). As discussed for the QD dispersions in the Supporting Information, insufficient ligand coverage can lead to accelerated trapping in solution. We speculate here that ligand density (partly) also explains the observed trend in the films: the diamine (2DA) and diacid (2DAc) ligands lead to a shorter lifetime than the dithiol ligands (2DT), in line with their smaller binding strengths.[9,25,26]

The TA spectra at 5 ps in Figure 2d reveal a broad photoinduced absorption (PA) feature below the band gap and extending to the infrared. This positive PA "shelf" feature is only seen for 2DA and 2DAc ligands and not for 2DT ligands. It is furthermore also observed for a dispersion with QDs of 3.7 nm diameter that featured a low PL quantum yield and fast trapping (see Figure S2b, Supporting Information). Its 1/e lifetime is typically hundreds of ps (see Figure S4, Supporting Information) and its magnitude seems to be related to a short lifetime of the $1S_{3/2}1S_e$ bleach, as it is hardly pronounced for 2DT ligands. This photoinduced absorption has been observed previously,[27−29] and was tentatively assigned to intraband transitions which receive oscillator strength from the presence of a trapped electron. The fact that this PA "shelf" feature is particularly pronounced for the films with 2DA and 2DAc ligands further suggests that trapping is significant in these films. Summarizing the results of Figure S2 (Supporting Information) and Figure 2, we find that electron trapping is efficient in CdTe QDs. Particularly the processing of QDs into photoconductive films leads to very efficient electron trapping.

Demonstration of Electron Transfer in CdTe-CdSe Multilayer Films. Next we investigate electron transfer between CdTe and CdSe QDs in QD films. We start by determining the bleach per excitation $\Delta A/(I_0 F_A)$ for 2DT capped single component films of 4.9 nm CdSe QDs (see Figure 3a) and 6.3 nm CdTe QDs (see Figure 3b). The CdSe QD film has been excited at 620 nm and the CdTe QD film at 670 nm. Both films exhibit a bleach maximum at their $1S_{3/2}1S_e$ transition, at 610 nm for CdSe and at 700 nm for CdTe, respectively. While also for the CdTe QD film the TA spectrum is nonzero at around 610 nm, the absorption changes are both positive and

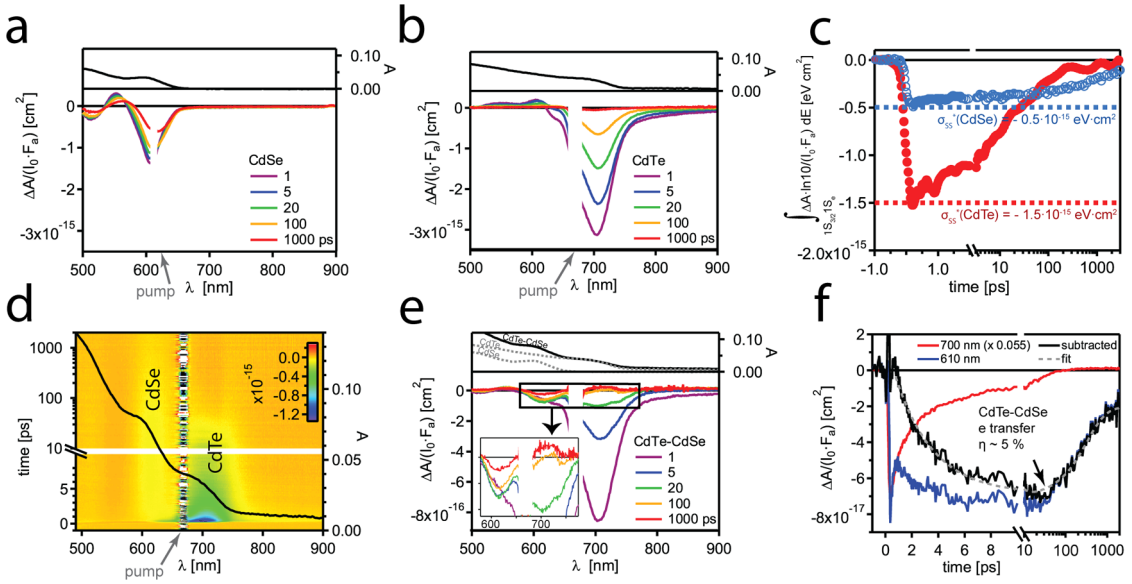

Figure 3. Demonstration of electron transfer from CdTe to CdSe QDs. TA spectra at selected pump-probe delays for films of 2DT capped 4.9 nm CdSe QDs (a) and 2DT capped 6.3 nm CdTe QDs (b). The spectral region around the pump wavelength shows significant pump scatter and is not shown. The linear absorption spectra are plotted as black solid lines *versus* the right axis. (c) Cross section per excitation σ_{SS}*, integrated over the $1S_{3/2}1S_e$ transition, for films of 2DT capped CdTe (red filled circles) and CdSe (blue open circles) QDs, respectively, as obtained from the measurements in (a) and (b), see main text. (d) 2D TA image displaying the bleach per excitation $\Delta A/(I_0F_A)$ for a QD solid comprising both 2DT capped CdSe QDs (4.9 nm) and 2DT capped CdTe QDs (6.3 nm) after selective excitation of the CdTe QDs at 670 nm. The linear absorption spectrum of the film is plotted as black solid line *versus* the right axis. The pump wavelength is indicated with a grey arrow. (e) Spectra of this film at selected pump-probe delays, along with its linear absorption spectrum and that of single layers of either CdSe or CdTe. The inset is a magnification of the spectral region marked by the black box. (f) Kinetics of the CdSe $1S_{3/2}1S_e$ (610 nm) and CdTe $1S_{3/2}1S_e$ (700 nm) transition for the measurement in (d). The black line displays the kinetics obtained by subtracting the kinetics at 700 nm (scaled by 0.055) from the kinetics at 610 nm. A fit consisting of a single-exponential ingrowth and a biexponential decay is shown as a grey dashed line.

negative and most likely result from spectral shifts rather than bleaches due to state-filling.[30] After integration over the region of the CdSe $1S_{3/2}1S_e$ transition (563 to 660 nm), the CdTe TA signal is negligible compared to the signal integrated over the region of the CdTe $1S_{3/2}1S_e$ transition (630 to 755 nm). This will facilitate the spectral assignment to either CdSe or CdTe in the films comprising both materials.

Before continuing with the composite films, we first quantify how much absorption bleach is produced by a single excitation. Figure 3c shows this quantity $\int_{1S_{3/2}1S_e}((\Delta A(E,t)\cdot \ln 10)/(I_0F_A))\,dE$ for single component films of CdTe QDs (red filled circles) and CdSe QDs (blue open circles), respectively, where the integration over the $1S_{3/2}1S_e$ transition has been introduced to average over all QDs in the ensemble and to account for spectral shifts. At time zero, this quantity equals $\sigma_{SS}^* \equiv \int_{1S_{3/2}1S_e}\sigma^*(E)\,dE$, the cross section per excitation as given in eq 2, integrated over the $1S_{3/2}1S_e$ transition. Note that the integration changes the unit of the resulting quantity to eV cm^2. In Figure 3c, the $1S_{3/2}1S_e$ integrated cross section is indicated by dashed lines, being larger for CdTe ($\sigma_{SS}^* = -1.5\cdot10^{-15}$ cm^2) than for CdSe ($\sigma_{SS}^* = -0.5\cdot10^{-15}$ cm^2). It may be compared to the $1S_{3/2}1S_e$ integrated linear absorption cross section per QD given in ref 19, where it was determined for QD dispersions. The latter is a factor 3.5 and 2.8 smaller than the section per excitation determined here for CdTe and CdSe, respectively. This indicates that the absorption cross section in the QD films studied here is somewhat larger than for QD dispersions. The higher dielectric constant of the film compared to dispersions, possibly results in a higher local field factor in the Maxwell–Garnet model resulting in an increase in absorption.[31]

Next, films of both donor (CdTe) and acceptor (CdSe) QDs were prepared in an alternating multilayer architecture: first approximately a monolayer of 4.9 nm CdSe QDs is deposited, followed by a monolayer of 6.3 nm CdTe QDs and this sequence is repeated 5 times. In between the QD depositions, the original ligands are exchanged to 2DT ligands, as these are (1) short enough to provide the necessary wave function overlap between donor and acceptor QDs and (2) are the ligands with the longest lifetimes in our single component films (see Figure 2e). Finally, the alternating multilayer ensures contact of each CdTe QD with CdSe QDs.[14]

CdTe QDs were excited selectively with pump pulses (670 nm) having sufficient energy to induce optical transitions across the band gap of CdTe (710 nm), but not CdSe (610 nm). After excitation, only the electron is expected to transfer from CdTe to CdSe QDs, while the hole should stay in CdTe QDs. Both the

2D TA image in Figure 3d and the spectra at selected pump-probe delays in Figure 3e show an instantaneous bleach at the CdTe $1S_{3/2}1S_e$ transition (around 700 nm) and a delayed bleach at the CdSe $1S_{3/2}1S_e$ transition (around 610 nm). Figure 3f displays the kinetics of both features, where the 700 nm feature has been scaled by a factor 0.055 for clarity. The decay at 700 nm can be attributed to depopulation of $1S_e$ electrons in CdTe. The bleach at 610 nm features an instantaneous rise at time zero, followed by an ultrafast decay within the first 0.5 ps. Subsequently, it increases again over 20 ps until it decays on a nanosecond time scale. These rich kinetics at 610 nm arise both from CdSe and CdTe QDs, as the smallest CdTe QDs have a minor spectral overlap with CdSe QDs (see Figure 3a,b). We attribute the initial rise and fast decay to small CdTe QDs as suggested by the similarity of the kinetics at 610 nm and the kinetics at 700 nm (scaled by a factor 0.055) during the first 0.5 ps. In contrast, the subsequent increase of the 610 nm bleach originates from a bleach of the $1S_{3/2}1S_e$ transition in CdSe, as inferred from the spectra in Figure 3e. This indicates an electron transfer process.

To extract the kinetics of electron transfer to CdSe from the signal at 610 nm, we subtract the scaled kinetics at 700 nm from the kinetics at 610 nm, depicted as a black line in Figure 3f. A fit consisting of a single-exponential ingrowth and a biexponential decay is shown as a grey dashed line. The time constants are $\tau_{CdSe,1} = 2.9 \pm 0.1$ ps for the ingrowth, and $\tau_{CdSe,2} = 327 \pm 20$ ps and $\tau_{CdSe,3} = 26$ ns for the decay, respectively, where $\tau_{CdSe,3}$ has been fixed at the radiative decay time of the CdSe QDs.[23] On the other hand, the CdTe bleach kinetics at 700 nm can be fitted with a biexponential decay with time constants $\tau_{CdTe,1} = 0.22 \pm 0.01$ ps and $\tau_{CdTe,2} = 2.4 \pm 0.1$ ps. The latter is very close to the ingrowth time constant $\tau_{CdSe,1}$. Hence, we assign $\tau_{CdSe,1}$ to electron transfer from the CdTe $1S_e$ to the CdSe $1S_e$ level. The $\tau_{CdTe,1}$ component is assigned to very efficient electron trapping in the CdTe QDs. Its value of 0.22 ps is likely limited by the instrumental time resolution and is hence an upper limit.

The electron transfer time found here is in line with the reported transfer time between CdSe QDs and SnO_2 of 3 ± 1 ps and 25 ± 2 ps, when separated by a molecular bridge slighter shorter (HS-CH_2-COOH) or longer (HS-$[CH_2]_3$-COOH) than ours.[4] It is also similar to reported electron transfer times in solution, 2 ps from CdSe QDs to methylene blue,[32] 2.3 ps from PbS QDs to methylene blue[32] or 3.8 ps from PbS QDs to 1,4-benzoquinone.[33] The component $\tau_{CdSe,2}$ (327 ps) is attributed to electron trapping in CdSe, as it is shorter than the radiative lifetime and there are no holes for Auger recombination in CdSe. Such relatively slow decay is also observed in the control experiment with CdSe QDs only (see Figure 3c). This further corroborates that electrons have arrived in CdSe QDs.

The efficiency of electron transfer η_{ET} from CdTe to CdSe QDs can be determined by comparing the observed absorption bleach of the CdSe $1S_{3/2}1S_e$ transition after electron transfer to the cross section per excitation σ_{SS}* in the single component CdSe QD film as determined above:

$$\eta_{ET} = \frac{\max\{-\int_{1S_{3/2}1S_e} \Delta A(E,t)\, dE\} \cdot \ln 10}{-\sigma_{SS}^* I_0 F_A} \quad (3)$$

The max function indicates that we take the highest value of the integrated transient absorption signal in the CdSe QD $1S_{3/2}1S_e$ spectral region (*i.e.*, the maximum of the bleach transient). As discussed above we assume that the bleach of the $1S_{3/2}1S_e$ is due to electrons only. In this case the hole (present in the determination of σ_{SS}*) may be neglected and eq 3 is valid. For the CdSe-CdTe QD film discussed here, a transfer efficiency of 5% is obtained. This low value is the result of the competition between electron transfer with a rate of $\sim (2.9\ \text{ps})^{-1}$ and very fast electron trapping in CdTe QDs with a rate of $\geq (0.22\ \text{ps})^{-1}$. A straightforward estimate of the transfer efficiency based on these rates gives $\eta_{ET} \leq (2.9)^{-1}/((2.9)^{-1} + (0.22)^{-1}) = 7.1\%$, in close agreement with the value of 5% obtained *via* eq 3.

Electrochemical Gating Controls Electron Trapping. While we have shown above that with 2DT ligands electron transfer from CdTe QDs to CdSe QDs may be observed, the transfer yield is low (5%) as electron trapping is faster than electron transfer. In the following, we attempt to eliminate electron trapping *via* electrochemical gating: we immerse a CdTe QD film on an ITO substrate in an electrochemical cell containing 0.1 M $LiClO_4$ in acetonitrile, a Ag pseudoreference electrode and a Pt counter electrode. The ITO substrate serves as a working electrode whose Fermi level can be changed in a controlled and reversible fashion by setting a voltage *versus* the calibrated Ag pseudoreference electrode (−4.7 V *versus* vacuum). Unless stated otherwise, all potentials mentioned hereafter are given with respect to this Ag pseudoreference electrode. Upon changing the potential, no charges are injected into the $1S_e$ electron level, as no steady state $1S_{3/2}1S_e$ bleach is observed.[34] However, electron traps may be filled. In fact, for CdTe QDs, injection of electrons into the $1S_e$ level is difficult, possibly as a result of a large number of traps within the band gap that need to be filled first.

Figure 4b shows a 2D TA image of a film of 6.3 nm CdTe QDs with 1,8-octanediamine (8DA) ligands on ITO, after photoexcitation at 460 nm. Longer ligands were chosen here as these facilitate cation uptake and result in more efficient charging.[34] The film was immersed in the electrochemical cell described above and held at open circuit potential. This situation is comparable to the conventional TA measurements on CdTe films in Figure 2. In agreement with Figure 2, the

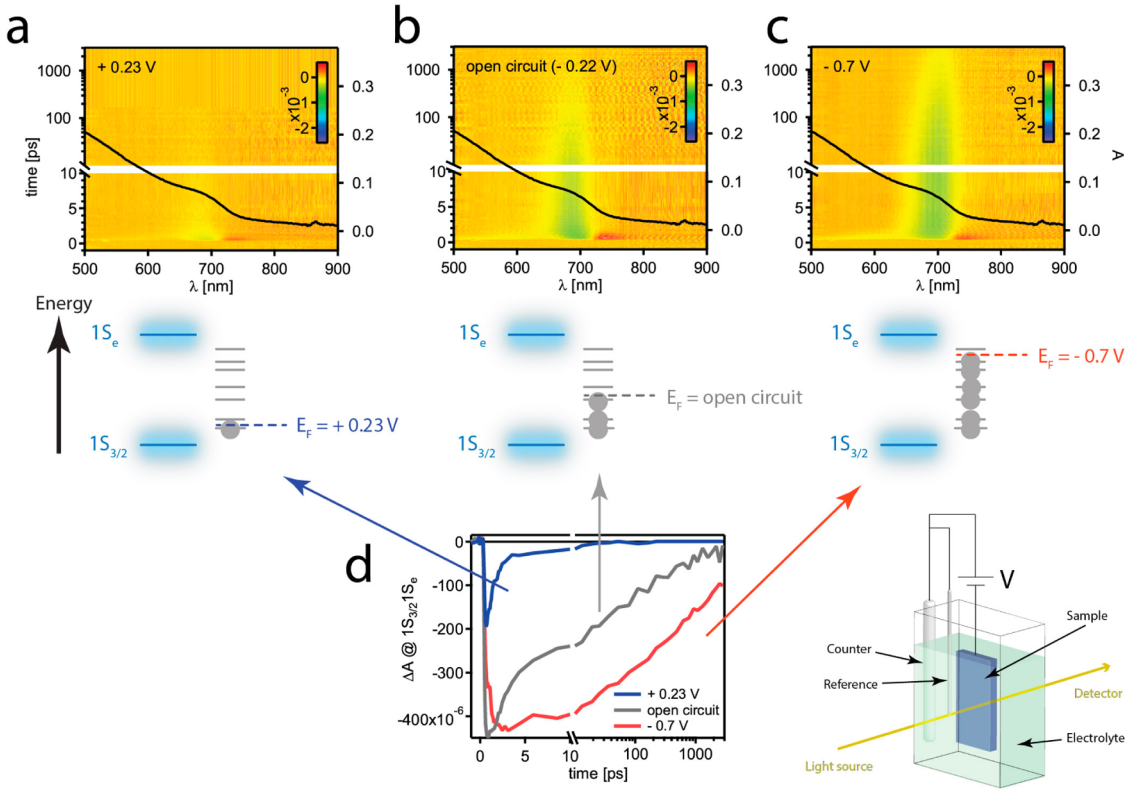

Figure 4. Switching off electron trapping. 2D TA image of a film of 6.3 nm CdTe QDs with 8DA ligands on an ITO substrate after 460 nm excitation (a) at +0.23 V *versus* Ag pseudoreference electrode, (b) at open circuit, corresponding to −0.22 V, and (c) at −0.7 V, respectively. (d) Kinetics of the $1S_{3/2}1S_e$ transition at 700 nm for all applied potentials. The schematic in the second row sketches the filling of traps states going from (a) to (c), using an electrochemical cell (lower right) to control the Fermi level.

1/e lifetime of the $1S_{3/2}1S_e$ bleach is 35 ps; the majority has decayed even within the first 5 ps, indicating fast electron trapping (see kinetic trace in Figure 4d). The decay is even faster when the Fermi level is moved to +0.23 V, *i.e.*, closer towards to $1S_{3/2}$ hole level (see Figure 4a,d): now, the 1/e lifetime has decreased to 1.4 ps. This accelerated decay is most likely also the reason why the maximum bleach is less than half that of the open circuit case: electrons get trapped within the time duration of the pump pulse. We attribute such fast decay to a higher electron trapping rate as more electron traps are unoccupied at +0.23 V. We now move the Fermi level towards the $1S_e$ level, to −0.7 V. In this case, a much slower decay of the $1S_{3/2}1S_e$ bleach is observed (see Figure 4c,d): the 1/e lifetime has increased to 1 ns. Hence, by raising the Fermi level by 1 V, we could slow down electron trapping by three orders of magnitude. Similar effects are also seen for other QD sizes as well as for dithiol ligands (1,6-hexanedithiol) and shorter diamine ligands (1,2-ethanediamine and 1,7-heptanediamine). Summarizing, the decay of the $1S_{3/2}1S_e$ bleach becomes slower when the Fermi level gets closer to the $1S_e$ level, a situation in which more electron traps are occupied and more hole traps are unoccupied. This corroborates our above assignment that the $1S_{3/2}1S_e$ bleach decay reflects electron (and not hole) trapping, as hole trapping would show the opposite effect, *i.e.*, it would be faster at −0.7 V than at +0.23 V.

One could argue that electron trapping may be induced by ultrafast hole trapping followed by rapid electron-hole recombination, rather than taking place on electron traps directly. The above results however show that this is not the case. In this scenario the $1S_{3/2}1S_e$ bleach decay would be governed by the availability of hole traps. This would lead to increased electron trapping when the Fermi level is raised closer to the $1S_e$ level as this leads to a higher number of available hole traps, opposite to the observation. Hence, we conclude that there is a large number of electron traps throughout the band gap that lead to fast electron trapping if they are empty, but that this trapping channel can be switched off by raising the Fermi level.

To the best of our knowledge, this is the first time that electrochemical control of the Fermi level has been combined with TA spectroscopy to identify, monitor and reduce trapping in QD films. Especially for samples in which trapping is a major decay channel, such as for our CdTe QDs, this technique offers a powerful method to study and control trapping. First, as the trapping rate depends on the density of trap states, it opens up the possibility to map the density of trap states (DOTS). Second, it improves the passivation of the QD surface and circumvents the

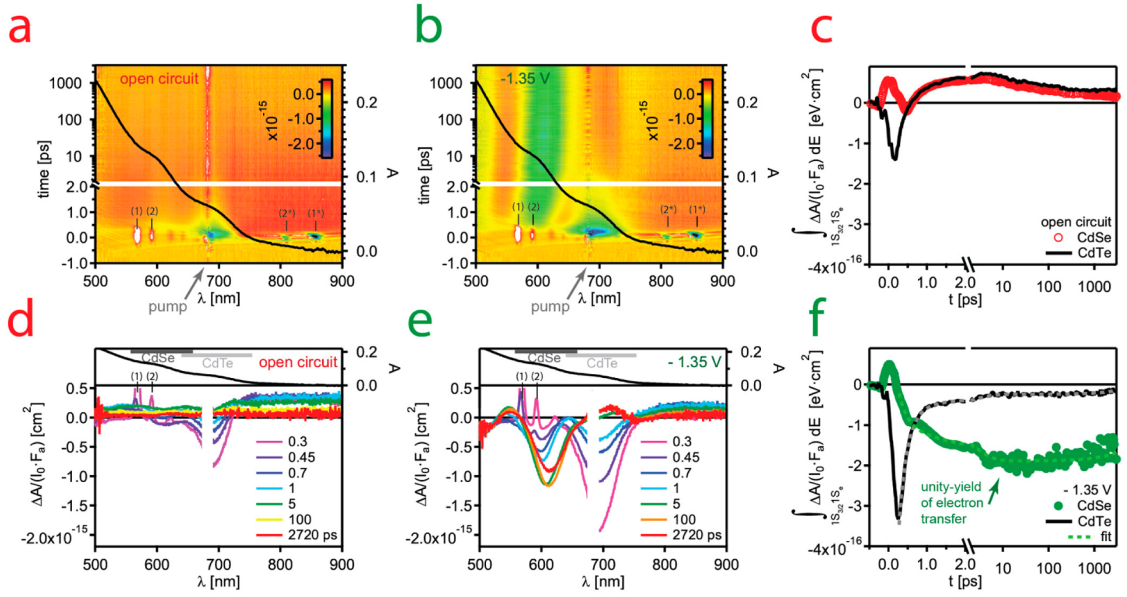

Figure 5. Electrochemistry enables charge transfer in a CdTe-CdSe QD film. Bleach per excitation $\Delta A/(I_0F_A)$ for a 2DA capped QD multilayer of both CdSe QDs (4.9 nm) and CdTe QDs (6.3 nm) on ITO after excitation at 680 nm, in an electrochemical cell containing 0.1 M $LiClO_4$ electrolyte. (a) 2D TA image at open circuit with the film's linear absorption spectrum plotted as black solid line *versus* the right axis. The pump wavelength is indicated with an arrow and Raman excitations of acetonitrile at time zero with labels (1), (2), (2*) and (1*). (b) 2D TA image after the film's Fermi level has been raised to −1.35 V *versus* Ag pseudoreference electrode. (d) and (e) display spectra at selected pump-probe delays, while (c) and (f) show the ingrowth and decay of the bleach per excitation for CdSe (circles) and CdTe (continuous lines), respectively, integrated over the $1S_{3/2}1S_e$ transition. The integration boundaries for CdSe and CdTe are indicated with dark grey and light grey boxes, respectively. Fits to the traces in (f) are displayed as dashed lines.

problem of achieving sufficient ligand coverage, a common challenge[35,36] due to, *e.g.*, the inherent dynamic character of the surface.[37]

Electrochemical Gating Enables Electron Transfer. In the following, we exploit the electrochemical control of the Fermi level to improve the yield of electron transfer from CdTe to CdSe QDs. Alternating multilayers of both CdSe QDs (4.9 nm) and CdTe QDs (6.3 nm) are deposited on ITO and the QD ligands are exchanged to 2DA. In an electrochemical cell containing a 0.1 M $LiClO_4$ in acetonitrile, CdTe QDs are selectively excited at 680 nm. Figure 5a shows the obtained 2D TA image at open circuit potential with the bleach per excitation $\Delta A/(I_0F_A)$ shown in false colors. At time zero, several spectrally narrow extrema appear which can be attributed to stimulated Raman excitations of acetonitrile.[38,39]

In addition, a short-lived bleach at the CdTe $1S_{3/2}1S_e$ transition (700 nm) and negligible signal at the CdSe $1S_{3/2}1S_e$ transition (610 nm) are seen. This is consistent with the previously observed fast electron trapping in CdTe QDs with 2DA ligands (see Figure 2a), which obstructs electron transfer to CdSe QDs. This is further illustrated by the kinetic traces in Figure 5c and the spectra at selected pump-probe delays in Figure 5d. Whereas the CdTe $1S_{3/2}1S_e$ bleach decays rapidly, it does not lead to a bleach at the CdSe $1S_{3/2}1S_e$ transition, at any pump-probe delay. In contrast, raising the Fermi level to −1.35 V leads to a bleach both at the CdTe and CdSe $1S_{3/2}1S_e$ transition (see Figure 5b). The $1S_{3/2}1S_e$ integrated bleach kinetics in Figure 5f show that the CdSe bleach is significant and appears simultaneously with the decay of the CdTe bleach.

A triexponential fit to the CdTe decay (grey dashed line) yields the time constants $\tau_{CdTe,1} = 0.23 \pm 0.01$ ps, $\tau_{CdTe,2} = 2.3 \pm 0.3$ ps and $\tau_{CdTe,3} = \tau_{rad} = 38.8$ ns. The CdSe kinetics are well-described with a biexponential ingrowth where the time constants $\tau_{CdSe,1} = \tau_{CdTe,1}$ and $\tau_{CdSe,2} = \tau_{CdTe,2}$ have been set to the respective CdTe decay constants, and a single-exponential decay with the radiative lifetime of CdSe QDs $\tau_{CdSe,3} = 26$ ns. The fit is displayed as the light green dashed line. The good agreement between the data and fits containing only the radiative lifetime and two time constants describing both the ingrowth of the CdSe bleach and the decay of the CdTe bleach suggests that electron trapping is negligible and $\tau_{CdSe,1} = \tau_{CdTe,1}$ and $\tau_{CdSe,2} = \tau_{CdTe,2}$ are electron transfer times. While the latter is comparable with the transfer time of 2.9 ± 0.1 ps in the CdTe-CdSe QD multilayer with 2DT ligands in conventional TA (see Figure 3 and Table 1), the former is very close to the ∼200 fs time resolution of the experiment, indicating an accelerated transfer channel. This fast transfer is in line with the magnitude of the CdTe bleach at early times, which is a factor 2 lower than expected from eq 2, using the excitation cross section of the single component CdTe QD film (see Figure 3f).

The transfer yield at −1.35 V is 95%, as determined *via* eq 3. Estimating a combined error of 20% in the

determination of the pump fluence and the CdSe QD excitation cross section, we conclude that the transfer yield is close to unity. This is corroborated by the fits of the kinetics (Figure 5e) that suggest that electron trapping is absent.

Thus, electrochemical control of the Fermi level clearly enables much higher electron transfer efficiencies than does exchanging the 2DA ligands for 2DT ligands (see Figure 3). As the rate of electron transfer is similar in both cases, one can attribute this to a reduction of the trapping rate in CdTe QDs. This is in line with the same finding for the single component films (see Figures 2 and 4) and consistent with the lack of trapping in the model to fit the CdTe bleach kinetics in Figure 5f. The absence of trapping in the fit to the CdSe bleach kinetics completes the picture: apparently, the rise of the Fermi level has also filled electron traps in CdSe and, hence, reduced the trapping rate in this material as well.

CONCLUSIONS AND OUTLOOK

In conclusion, electron trapping is a common process in CdTe QDs. Broadband TA measurements in dispersion reveal that the lifetime of the $1S_{3/2}1S_e$ bleach depends on the QD surface quality, which is affected by, *e.g.*, the purification protocol after synthesis. In films with short bidentate ligands, electron trapping is further accelerated with amines and acids leading to considerable trapping even within the duration of the exciting laser pulse (< 0.2 ps). Using thiol ligands, trapping can be slowed down. This allows electron transfer to CdSe QDs, which form a type II band offset with CdTe QDs. However, the yield of electron transfer is low (5%) as electron trapping is still faster than electron transfer. Using a novel combination of electrochemical gating and TA, we show that electrochemical control of the Fermi level in CdTe QD films decreases the trapping rate by three orders of magnitude. This leads to an efficiency of electron transfer from CdTe to CdSe QDs of close to unity. We propose that this method can also be applied to other materials, offering facile and reversible control of the Fermi level. It opens up the possibility of studying the density of trap states (DOTS) as well as the systematic investigation of electron transfer without the complication of trapping.

EXPERIMENTAL SECTION

Materials. 1,2-Ethanediamine (99.5%, Fluka); 1,2-ethanedithiol (98%, Fluka); oxalic acid (anhydrous, 99%, Sigma-Aldrich); 1,8-octanediamine (98%, Aldrich); methanol (anhydrous, 99.8%, Sigma-Aldrich); butanol (anhydrous, 99.8%, Sigma-Aldrich); acetonitrile (anhydrous, 99.8%, Sigma-Aldrich); $LiClO_4$ (battery grade, dry, 99.99%, Aldrich); Se (325 mesh, 99.99%, ChemPur); Te (−18+60 mesh, 99.999%, Alfa Aesar); $Cd(Ac)_2$ (anhydrous, 99.999%, Strem Chemicals); trioctylphosphine (97%, Aldrich); trioctylphosphine oxide (99%, Aldrich); 1-hexadecylamine (technical grade, 90%, Alfa Aesar); 1-tetradecylphosphonic acid (98%, Alfa Aesar); 1-octadecene (technical grade, 90%, Aldrich); oleic acid (technical grade, 90%, Aldrich). All materials were used as received.

QD Synthesis. CdSe QDs with 4.9 nm diameter were synthesized following the recipe by Mekis *et al.*:[16] two precursors were prepared in a N_2 purged glove box by dissolving 0.474 g Se (325 mesh) in 6 mL of TOP (trioctylphosphine) and 0.36 g of $Cd(Ac)_2$ in 9 mL of TOP, respectively. Subsequently, the synthesis was done in a Schlenk line providing oxygen- and water-free conditions. 24 g of TOPO (trioctylphosphine oxide) was heated to 180 °C in a vacuum under periodic flushing with N_2. After cooling down to 100 °C, 15 g of HDA (1-hexadecylamine) and 0.45 g of TDPA (1-tetradecylphosphonic acid) were added and dried at 120 °C in a vacuum during 30 min under periodic flushing with N_2. The TOP-Se precursor was injected and the solution was heated to 300 °C under N_2 flow. Under vigorous stirring, the TOP-$Cd(Ac)_2$ precursor was injected to induce nucleation of CdSe nanoparticles. After growth at 280 °C, the reaction was stopped by injection of cold toluene and external cooling. The obtained dispersion was purified by repeated washing with anhydrous MeOH and precipitation of particles in a centrifuge at 3000 rpm for 5 min. The final stock of particles was dispersed in Chloroform.

We synthesized CdTe QD dispersions with diameters of 3.7 and 6.3 nm, respectively, following the procedure described by Kloper *et al.*[40] At 310 °C in N_2 atmosphere, a TOP-Te precursor in ODE (octadecene) is injected rapidly to a Cd-$(oleate)_2$ precursor in ODE under vigorous stirring. Growth took place at 270 °C and was stopped after several minutes by injection of cold toluene. The dispersions were purified as follows: anhydrous MeOH and anhydrous BuOH were added as nonsolvents to precipitate the QDs in a centrifuge at 3500 rpm during 7 min. Typically, the volume ratio was 1:1:2 (reaction solution:MeOH:BuOH). Subsequently, the precipitate was redispersed in chloroform and the whole purification procedure was repeated once.

Film Processing and Ligand Exchange. Films for electrochemical studies are deposited on an ITO substrate; all other films are deposited on a quartz substrate. Films with either 2DT, 2DAc, 2DA or 8DA ligands are grown in a layer-by-layer (LbL) dip coating procedure in a N_2 purged glove box: the substrates were first immersed for 30 s in a concentrated QD dispersion, subsequently immersed for 30 s in a stirred 1 M solution of the desired ligand in MeOH, and finally dipped twice for 10s in stirred MeOH to rinse excess ligands. Using this procedure, the original insulating ligands are replaced by the shorter bidentate ligands. The above procedure was repeated 10−20 times to yield films roughly 10−20 QD monolayers thick. In CdTe-CdSe multilayer films, the substrates were alternatively dipped in CdTe and CdSe QD dispersions. For electrochemical measurements, a small region on the edge of the ITO substrate remained uncoated to provide electrical contact.

Broadband Transient Absorption Measurements. Broadband transient absorption (TA) measurements were performed on either QD dispersions in chloroform in a 2 mm cuvette or on films on a quartz substrate in an air-tight cell containing N_2. Optical densities were typically between 0.05 and 0.2 to provide uniform excitation densities. Samples were excited with ∼200 fs pump pulses from an OPA (Light Conversion ORPHEUS) after a regenerative amplifier (Light Conversion PHAROS), at a repetition rate of 2500 Hz. Absorption spectra in the visible (450−900 nm) were recorded with an Ultrafast Systems HELIOS spectrometer at a repetition rate of 5000 Hz using broadband probe pulses from a sapphire crystal pumped by 1030 nm. A variable delay of −10 to 3000 ps between probe and pump pulses was introduced to yield difference absorption spectra, as a function of pump−probe delay and probe energy. Because of dispersion in optical components between the white light generating crystal and the photodetector, the "time zero", *i.e.*, the point of time where pump and probe show maximum temporal overlap, depends on the probe wavelength. Dispersion corrected 2D TA data with

identical time zero for all wavelengths were obtained by subtracting a third-order polynomial fit to the "coherent artifact"[41,42] from the raw data. About 10 000 difference absorption spectra were obtained per pump−probe delay.

Electrochemical Control of the Fermi Level. The Fermi level of our QD films on ITO was controlled by a CHI832B bipotentiostat (CH Instruments, Inc.), while immersed in an airtight glass container with an Ag wire pseudoreference electrode and a Pt sheet counter electrode (see inset in Figure 4). The Ag wire pseudoreference electrode (−4.7 V *versus* vacuum) was calibrated with a ferrocene/ferrocinium couple. In a N_2 purged glove box, the cell is loaded with a QD film and filled with an electrolytes consisting of anhydrous acetonitrile and 0.1 M $LiClO_4$ (lithium perchlorate). All chemicals were used as received. The electrochemical cell is placed such that TA measurements are possible, with both pump and probe beams passing through the front window, the QD films and the back window of the cell. For all applied potentials reported in the main text, care was taken that the absorption of the unexcited sample did not change with respect to open circuit potential. Hence, no charges were injected into quantum confined levels.

Conflict of Interest: The authors declare no competing financial interest.

Acknowledgment. We thank L. T. Kunneman and W. H. Evers for helpful discussions. This work is part of the Joint Solar Programme (JSP) of HyET Solar and the Stichting voor Fundamenteel Onderzoek der Materie (FOM), which is part of The Netherlands Organisation for Scientific Research (NWO).

Supporting Information Available: Dispersion correction of transient absorption data. Transient absorption measurements featuring the effect of washing of QD dispersion, the effect of excitation energy, an example of the photoinduced absorption "shelf" signal, and the determination of the excitation cross section. Estimation of band alignment for CdSe and CdTe QDs. This material is available free of charge *via* the Internet at http://pubs.acs.org.

Note Added after ASAP Publication: This paper published ASAP on June 5, 2014. After publication, corrections were made to equations 1, 2, and 3, Figure 3, and discussion of absorption bleach in the section entitled Demonstration of Electron Transfer in CdTe-CdSe Multilayer Films, including addition of reference 31. Supporting Information was corrected accordingly. The revised article and SI were reposted on June 19, 2014.

REFERENCES AND NOTES

1. Nozik, A. J. Quantum Dot Solar Cells. *Physica E* **2002**, *14*, 115–120.
2. Wright, M.; Uddin, A. Organic—Inorganic Hybrid Solar Cells: A Comparative Review. *Sol. Energy Mater. Sol. Cells* **2012**, *107*, 87–111.
3. Tvrdy, K.; Frantsuzov, P. A.; Kamat, P. V. Photoinduced Electron Transfer from Semiconductor Quantum Dots to Metal Oxide Nanoparticles. *Proc. Natl. Acad. Sci. U. S. A.* **2010**, *108*, 29–34.
4. Wang, H.; McNellis, E. R.; Kinge, S.; Bonn, M.; Cánovas, E. Tuning Electron Transfer Rates through Molecular Bridges in Quantum Dot Sensitized Oxides. *Nano Lett.* **2013**, *13*, 5311–5315.
5. Yang, Y.; Rodríguez-Córdoba, W.; Xiang, X.; Lian, T. Strong Electronic Coupling and Ultrafast Electron Transfer between PbS Quantum Dots and TiO_2 Nanocrystalline Films. *Nano Lett.* **2012**, *12*, 303–309.
6. Zhu, H.; Song, N.; Lian, T. Controlling Charge Separation and Recombination Rates in CdSe/ZnS Type I Core−Shell Quantum Dots by Shell Thicknesses. *J. Am. Chem. Soc.* **2010**, *132*, 15038–15045.
7. Hyun, B.-R.; Zhong, Y.-W.; Bartnik, A. C.; Sun, L.; Abruña, H. D.; Wise, F. W.; Goodreau, J. D.; Matthews, J. R.; Leslie, T. M.; Borrelli, N. F. Electron Injection from Colloidal PbS Quantum Dots into Titanium Dioxide Nanoparticles. *ACS Nano* **2008**, *2*, 2206–2212.
8. Morris-Cohen, A. J.; Frederick, M. T.; Cass, L. C.; Weiss, E. A. Simultaneous Determination of the Adsorption Constant and the Photoinduced Electron Transfer Rate for a CdS Quantum Dot−Viologen Complex. *J. Am. Chem. Soc.* **2011**, *133*, 10146–10154.
9. Pijpers, J. J. H.; Koole, R.; Evers, W. H.; Houtepen, A. J.; Boehme, S.; de Mello Donega, C.; Vanmaekelbergh, D.; Bonn, M. Spectroscopic Studies of Electron Injection in Quantum Dot Sensitized Mesoporous Oxide Films. *J. Phys. Chem. C* **2010**, *114*, 18866–18873.
10. Tisdale, W. A.; Zhu, X.-Y. Artificial Atoms on Semiconductor Surfaces. *Proc. Natl. Acad. Sci. U. S. A.* **2011**, *108*, 965–970.
11. Wei, S.-H.; Zhang, S. B.; Zunger, A. First-Principles Calculation of Band Offsets, Optical Bowings, and Defects in CdS, CdSe, CdTe, and Their Alloys. *J. Appl. Phys.* **2000**, *87*, 1304–1311.
12. Gross, D.; Mora-Seró, I.; Dittrich, T.; Belaidi, A.; Mauser, C.; Houtepen, A. J.; Como, E. D.; Rogach, A. L.; Feldmann, J. Charge Separation in Type II Tunneling Multilayered Structures of CdTe and CdSe Nanocrystals Directly Proven by Surface Photovoltage Spectroscopy. *J. Am. Chem. Soc.* **2010**, *132*, 5981–5983.
13. Wang, Y.; Wang, L.; Waldeck, D. H. Electrochemically Guided Photovoltaic Devices: A Photocurrent Study of the Charge Transfer Directionality between CdTe and CdSe Nanoparticles. *J. Phys. Chem. C* **2011**, *115*, 18136–18141.
14. Talgorn, E.; de Vries, M. A.; Siebbeles, L. D. A.; Houtepen, A. J. Photoconductivity Enhancement in Multilayers of CdSe and CdTe Quantum Dots. *ACS Nano* **2011**, *5*, 3552–3558.
15. Kloper, V.; Osovsky, R.; Kolny-Olesiak, J.; Sashchiuk, A.; Lifshitz, E. The Growth of Colloidal Cadmium Telluride Nanocrystal Quantum Dots in the Presence of Cd^0 Nanoparticles. *J. Phys. Chem. C* **2007**, *111*, 10336–10341.
16. Mekis, I.; Talapin, D. V.; Kornowski, A.; Haase, M.; Weller, H. One-Pot Synthesis of Highly Luminescent CdSe/CdS Core−Shell Nanocrystals *via* Organometallic and "Greener" Chemical Approaches. *J. Phys. Chem. B* **2003**, *107*, 7454–7462.
17. Gao, Y.; Aerts, M.; Sandeep, C. S. S.; Talgorn, E.; Savenije, T. J.; Kinge, S.; Siebbeles, L. D. A.; Houtepen, A. J. Photoconductivity of PbSe Quantum-Dot Solids: Dependence on Ligand Anchor Group and Length. *ACS Nano* **2012**, *6*, 9606–9614.
18. Klimov, V. I. Optical Nonlinearities and Ultrafast Carrier Dynamics in Semiconductor Nanocrystals. *J. Phys. Chem. B* **2000**, *104*, 6112–6123.
19. Kambhampati, P. Hot Exciton Relaxation Dynamics in Semiconductor Quantum Dots: Radiationless Transitions on the Nanoscale. *J. Phys. Chem. C* **2011**, *115*, 22089–22109.
20. Efros, A. L.; Rodina, A. V. Band-Edge Absorption and Luminescence of Nonspherical Nanometer-Size Crystals. *Phys. Rev. B: Condens. Matter Mater. Phys.* **1993**, *47*, 10005–10007.
21. Morris-Cohen, A. J.; Donakowski, M. D.; Knowles, K. E.; Weiss, E. A. The Effect of a Common Purification Procedure on the Chemical Composition of the Surfaces of CdSe Quantum Dots Synthesized with Trioctylphosphine Oxide. *J. Phys. Chem. C* **2009**, *114*, 897–906.
22. Talgorn, E.; Moysidou, E.; Abellon, R. D.; Savenije, T. J.; Goossens, A.; Houtepen, A. J.; Siebbeles, L. D. A. Highly Photoconductive CdSe Quantum-Dot Films: Influence of Capping Molecules and Film Preparation Procedure. *J. Phys. Chem. C* **2010**, *114*, 3441–3447.
23. de Mello Donegá, C.; Koole, R. Size Dependence of the Spontaneous Emission Rate and Absorption Cross Section of CdSe and CdTe Quantum Dots. *J. Phys. Chem. C* **2009**, *113*, 6511–6520.
24. Klimov, V. I.; Mikhailovsky, A. A.; McBranch, D. W.; Leatherdale, C. A.; Bawendi, M. G. Quantization of Multiparticle Auger Rates in Semiconductor Quantum Dots. *Science* **2000**, *287*, 1011–1013.
25. Fritzinger, B.; Moreels, I.; Lommens, P.; Koole, R.; Hens, Z.; Martins, J. C. *In Situ* Observation of Rapid Ligand Exchange

in Colloidal Nanocrystal Suspensions Using Transfer NOE Nuclear Magnetic Resonance Spectroscopy. *J. Am. Chem. Soc.* **2009**, *131*, 3024–3032.
26. Koole, R.; Schapotschnikow, P.; de Mello Donegá, C.; Vlugt, T. J. H.; Meijerink, A. Time-Dependent Photoluminescence Spectroscopy as a Tool to Measure the Ligand Exchange Kinetics on a Quantum Dot Surface. *ACS Nano* **2008**, *2*, 1703–1714.
27. Malko, A. V.; Mikhailovsky, A. A.; Petruska, M. A.; Hollingsworth, J. A.; Klimov, V. I. Interplay between Optical Gain and Photoinduced Absorption in CdSe Nanocrystals. *J. Phys. Chem. B* **2004**, *108*, 5250–5255.
28. McArthur, E. A.; Morris-Cohen, A. J.; Knowles, K. E.; Weiss, E. A. Charge Carrier Resolved Relaxation of the First Excitonic State in CdSe Quantum Dots Probed with Near-Infrared Transient Absorption Spectroscopy. *J. Phys. Chem. B* **2010**, *114*, 14514–14520.
29. Saari, J. I.; Dias, E. A.; Reifsnyder, D.; Krause, M. M.; Walsh, B. R.; Murray, C. B.; Kambhampati, P. Ultrafast Electron Trapping at the Surface of Semiconductor Nanocrystals: Excitonic and Biexcitonic Processes. *J. Phys. Chem. B* **2012**, *117*, 4412–4421.
30. Trinh, M. T.; Houtepen, A. J.; Schins, J. M.; Hanrath, T.; Piris, J.; Knulst, W.; Goossens, A. P. L. M.; Siebbeles, L. D. A. In Spite of Recent Doubts Carrier Multiplication Does Occur in PbSe Nanocrystals. *Nano Lett.* **2008**, *8*, 1713–1718.
31. Moreels, I.; Lambert, K.; De Muynck, D.; Vanhaecke, F.; Poelman, D.; Martins, J. C.; Allan, G.; Hens, Z. Composition and Size-Dependent Extinction Coefficient of Colloidal PbSe Quantum Dots. *Chem. Mater.* **2007**, *19*, 6101–6106.
32. Zhu, H.; Yang, Y.; Lian, T. Multiexciton Annihilation and Dissociation in Quantum Confined Semiconductor Nanocrystals. *Acc. Chem. Res.* **2012**, *46*, 1270–1279.
33. Knowles, K. E.; Malicki, M.; Weiss, E. A. Dual-Time Scale Photoinduced Electron Transfer from PbS Quantum Dots to a Molecular Acceptor. *J. Am. Chem. Soc.* **2012**, *134*, 12470–12473.
34. Boehme, S. C.; Wang, H.; Siebbeles, L. D. A.; Vanmaekelbergh, D.; Houtepen, A. J. Electrochemical Charging of CdSe Quantum Dot Films: Dependence on Void Size and Counterion Proximity. *ACS Nano* **2013**, *7*, 2500–2508.
35. Morris-Cohen, A. J.; Malicki, M.; Peterson, M. D.; Slavin, J. W. J.; Weiss, E. A. Chemical, Structural, and Quantitative Analysis of the Ligand Shells of Colloidal Quantum Dots. *Chem. Mater.* **2012**, *25*, 1155–1165.
36. Anderson, N. C.; Owen, J. S. Soluble, Chloride-Terminated CdSe Nanocrystals: Ligand Exchange Monitored by ^{1}H and ^{31}P NMR Spectroscopy. *Chem. Mater.* **2012**, *25*, 69–76.
37. McBride, J. R.; Pennycook, T. J.; Pennycook, S. J.; Rosenthal, S. J. The Possibility and Implications of Dynamic Nanoparticle Surfaces. *ACS Nano* **2013**, *7*, 8358–8365.
38. Kovalenko, S. A.; Dobryakov, A. L.; Ruthmann, J.; Ernsting, N. P. Femtosecond Spectroscopy of Condensed Phases With Chirped Supercontinuum Probing. *Phys. Rev. A: At., Mol., Opt. Phys.* **1999**, *59*, 2369–2384.
39. The extrema labeled (1) and (1*) can be attributed to CH stretch vibrations (2950 cm^{-1}) and the extrema (2) and (2*) to CN stretch vibrations (2250 cm^{-1}).
40. Kloper, V.; Osovsky, R.; Kolny-Olesiak, J.; Sashchiuk, A.; Lifshitz, E. The Growth of Colloidal Cadmium Telluride Nanocrystal Quantum Dots in the Presence of Cd^{0} Nanoparticles. *J. Phys. Chem. C* **2007**, *111*, 10336–10341.
41. Lebedev, M. V.; Misochko, O. V.; Dekorsy, T.; Georgiev, N. On the Nature of "Coherent Artifact". *J. Exp. Theor. Phys.* **2005**, *100*, 272–282.
42. Dietzek, B.; Pascher, T.; Sundström, V.; Yartsev, A. Appearance of Coherent Artifact Signals in Femtosecond Transient Absorption Spectroscopy in Dependence on Detector Design. *Laser Phys. Lett.* **2007**, *4*, 38–43.